POLITECNICO DI TORINO
Repository ISTITUZIONALE

Free Vibrations of Damaged Aircraft Structures by Component-Wise Analysis

Original
Free Vibrations of Damaged Aircraft Structures by Component-Wise Analysis / Carrera, Erasmo; Pagani, Alfonso; Petrolo, Marco. - In: AIAA JOURNAL. - ISSN 0001-1452. - STAMPA. - 54:10(2016), pp. 3091-3106. [10.2514/1.J054640]

Availability:
This version is available at: 11583/2654679 since: 2020-04-24T15:55:14Z

Publisher:
American Institute of Aeronautics and Astronautics

Published
DOI:10.2514/1.J054640

Terms of use:

This article is made available under terms and conditions as specified in the corresponding bibliographic description in the repository

Publisher copyright

(Article begins on next page)

12 October 2024

Free vibrations of damaged aircraft structures by component-wise analysis

E. Carrera[1], A. Pagani[2], and M. Petrolo[3]

Department of Mechanical and Aerospace Engineering,

Politecnico di Torino, Corso Duca degli Abruzzi 24, 10129 Torino, Italy

By adopting advanced beam models, this paper presents free vibration analyses of metallic aircraft structures affected by local damages. Refined theories are developed within the framework of the Carrera Unified Formulation (CUF), according to which any order 2D and 1D theories of structures can be implemented in a hierarchical and unified manner. By employing Lagrange polynomials to expand the generalized displacement field, Component-Wise (CW) models of aircraft structures are implemented in this work. The CW approach provides a detailed physical description of multi-component structures since each component can be modelled with its own geometrical and mechanical characteristics, that is, no reference surfaces and axes and no homogenization techniques are employed. This characteristic allows us to model accurately global and local damages within the structure. The results show that the proposed refined 1D models can deal with the free vibration analysis of damaged aircraft structures as accurately as the shell and solid models. Moreover, thanks to the computational efficiency of CUF, CW models are good candidates for providing the vibration characteristics of structures for a wide range of damage scenarios in order to create databases able, for example, to train neural network for damage detection.

[1] Professor of Aerospace Structures and Aeroelasticity, and AIAA Member. E-mail: erasmo.carrera@polito.it
[2] Research Fellow. E-mail: alfonso.pagani@polito.it
[3] Research Fellow. E-mail: marco.petrolo@polito.it

Nomenclature

d	Impairment factor
E	Elastic modulus
F_τ	cross-section functions
G	shear modulus
$\mathbf{K}^{ij\tau s}$	fundamental nucleus of the elemental stiffness matrix
L	dimension of the structure in the y direction
L_{ext}	work of external loadings
L_{ine}	work of inertial loadings
L_{int}	strain energy
M	number of expansion terms
$\mathbf{M}^{ij\tau s}$	fundamental nucleus of the elemental mass matrix
N	expansion order for TE models
N_i	one-dimensional shape functions
p	polynomial order of the shape functions
$\mathbf{q}$	vector of the nodal generalized displacements
r, s	natural coordinates
r_τ, s_τ	natural coordinates of the Lagrange points
$\mathbf{u}$	three-dimensional displacements vector
$\mathbf{u}_\tau$	generalized displacements vector
u_x, u_y, u_z	three-dimensional displacement components
u_{x1}, u_{y1}, u_{z1},u_{x2}, ..., u_{zM}	generalized displacement components
V	beam volume ($V = \Omega \times L$)
$(x,\ y,\ z)$	coordinates reference system
δ	virtual variation
$\boldsymbol{\epsilon}$	strain vector
λ	Lame's parameter
ρ	material density

ν	Poisson ratio
$\boldsymbol{\sigma}$	stress vector
Ω	cross-section domain

I. Introduction

Damage detection in aircraft structures is of primary interest. Because of economical reasons, in aircraft maintenance programme, non-destructive testing (NDT) has acquired a predominant role. These include visual inspection, magnetic field tests and ultrasound. However, the modern NDT techniques require an estimation of the damage location before performing the test. To overcome this limitation, the evaluation of the modal characteristics through in situ measurements can be used to detect structural damages [1, 2]. As well-known, in fact, the presence of damages affects the vibration characteristics of a structure, and this has been exploited to develop damage detection techniques in many works. Some of the most recent papers on this topic are presented hereinafter. Zhang et al. [3] have proposed a graphical technique to detect the location and severity of delamination in composite beams by studying the frequency shifts induced by such damages. Capozucca [4] has studied the vibration response of damaged Carbon Fibre Reinforced Polymer (CFRP) beams. Pérez et al. [5] have conducted an extensive experimental activity to investigate the effects of damages on the vibrations of composite laminates. Wang et al. [6] have proposed a method for the damage detection and diagnosis in wind turbine blades that is based on the FEM dynamic analysis and the variation of the modal shape curvatures. Labib et al. [7] have studied the free vibrations of frames with multiple cracks by using the dynamic stiffness method and by modelling the cracks with rotational springs. Nguyen [8] has utilized 3D beam elements to calculate the mode shapes for damage detection of a cracked beam with a rectangular cross-section. Pollayi and Yu [9] have recently investigated the effects of the first damage mode (i.e., matrix micro-cracking) on the mechanical behaviour of helicopter rotor or wind turbine blades by modelling each blade as a beam based on geometrically nonlinear 3D elasticity theory and by employing VABS (Variational Asymptotic Beam Sectional Analysis) [10] and GEBT (Geometrically Exact Beam Theory) [11].

It is clear that the determination of the presence of damage, the quantification of the damage, the detection of the position of the damage, and the estimation of the remaining service life of the structure through free vibrations measurements requires the availability of databases including information about natural frequencies and mode shapes for a wide spectrum of damage cases. These databases can be provided by mathematical modelling and modal analysis of the structure under consideration. However, it should be underlined that this approach for damage detection presumes accurate and reliable measurements of the normal modes and frequencies through in situ tests. This aspect, although being rather questionable due to the lack of repeatability of the experiments even under very well controlled conditions, is out of the scope of this paper and further details can be found in [5].

Computational models for the analysis of damaged structures should be able to provide very accurate displacement and strain/stress fields. Damages may lead, in fact, to local and non-classical effects that require 3D-like analysis capabilities. Thus, classical Finite Element Method (FEM) models that make use of a combination of 2D and 1D elements for the analysis of reinforced-shell aircraft structures (see for example [12–14]) are not suitable. Currently, most of the techniques that have been developed for these tasks are based on very cumbersome numerical models, such as the 3D solid finite elements. In this paper, refined 1D beam finite elements are proposed and used to conduct free vibration analyses of damaged aircraft structures. It is obvious that classical beam theories, such as Euler-Bernoulli (EBBM) [15] or Timoshenko Beam Model (TBM) [16], are not suitable for damage detection. Many methods have been proposed over the last decades to enhance classical theories and to extend the application of 1D models to any geometry or boundary condition and mechanical complexity. A short review on some important advanced beam models is given below. For a more comprehensive discussion about recent developments in 1D models, the readers are referred to [17].

Some of the first proposed approaches to overcome the limitations of classical models were based on the introduction of shear correction factors, as in the works by Timoshenko [16, 18, 19], Sokolnikoff [20] and Cowper [21]. The introduction of warping functions to improve the displacement field of beams is another well-known strategy. Warping functions were first introduced in the framework

of the Saint Venant torsion problem [20]. Some of the earliest contributions to this approach were those by Umanskij [22], Vlasov [23] and Benscoter [24]. More recently, in the approach developed by Ladevéze and his co-workers [25], 3D elasticity equations were reduced to beam-like structures by describing the kinematics as the sum of a Saint Venant part and a residual part. Other important contributions related to one-dimensional structural modelling are those based on the Variational Asymptotic Method (VAM) and the Generalized Beam Theory (GBT). The work by Berdichevsky [26] was among the earliest contributions that exploited the VAM. Some valuable contributions on asymptotic methods are those related to VABS models, as in [27–30]. The GBT has been derived from Schardt's work [31–33]. The GBT enhances classical theories by exploiting a piece-wise description of thin-walled sections. It has been employed extensively and extended, in various forms, by Silvetre and Camotim and their co-workers, see for example [34]. In the framework of the beam modeling for design of helicopter blades, wind turbine blades, and high-aspect-ratio wings, it is important to mention the seminal work by Giavotto et al. [35] and the subsequent contributions of the authors. Many other higher-order theories, based on enhanced displacement fields over the beam cross-section, have been introduced to include non-classical effects. Some considerations on higher-order beam theories were made by Washizu [36]. Other refined beam models can be found in the review by Kapania and Raciti [37, 38], which focused on bending, vibration, wave propagations, buckling and post-buckling.

This work exploits the Carrera Unified Formulation (CUF) for higher-order 1D models [39, 40]. In CUF models, the displacement field above the cross-section is modelled through expansion functions whose order is a free parameter of the analysis. In other words, any-order structural models can be implemented with no need for formal changes in the problem equations and matrices. CUF can, therefore, deal with arbitrary geometries, boundary conditions and material characteristics with no need for ad hoc formulations. The most recent extension of CUF models is the so-called Component-Wise approach (CW). The CW is based on the use of Lagrange polynomials for the cross-section displacement field description [41] and it allows for multi-component structures to be modelled through a unique 1D formulation. Recently, the CW approach was used for the analysis of aerospace [42–44], civil engineering [45, 46] and laminated composite structures [47, 48], where it

was demonstrated that 1D CW leads to solid-like accuracies with far less computational costs than the shell and solid FEs.

In this paper, by employing CW models, the free vibration characteristics of damaged metallic aircraft structures are discussed by natural frequencies tracking and mode shapes changes. In particular, the Modal Assurance Criterion (MAC) is used to characterize mode variations between undamaged and damaged structures. MAC is defined as a scalar representing the degree of consistency between two distinct modal vectors [49]. It takes on values from zero (representing no consistent correspondence), to one (representing a consistent correspondence). Salawu and Williams [50] exploited the MAC and Coordinate Modal Assurance Criterion (COMAC) for the damage analysis of bridges. More recent papers on the same topic are those by Zhao and Zhang [51], Mukhopadhyay et al. [52], Balsamo et al. [53]. A comprehensive and detailed description of the main computational tools for damage detection can be found in the book of Gopalakrishnan et al. [54].

The present paper is organized as follows: first one-dimensional CUF models are introduced; then, CW and damage modelling is discussed; subsequently, numerical discussions of simple longeron to complex wing structures are provided; finally, the main conclusions are drawn.

II. One-dimensional refined models

In the case of slender, solid-section, homogeneous structures subject to bending phenomena, classical beam models (e.g., EBBM and TBM) provide a reasonably good approximation of the problem. On the other hand, it is obvious that for damage detection and accurate free vibration analysis of damaged structures theories able to deal with local phenomena and 3D strain effects are needed. Refined beam models can fulfill this requirement and, if sufficiently enriched kinematics is adopted, they can provide the same accuracy of 3D elasticity solutions with very low computational costs. In this paper, the Carrera Unified Formulation (CUF) is employed to automatically develop 1D refined models with an arbitrary number of terms in the kinematic field. The basic ideas and the main advantages of CUF are described in this section.

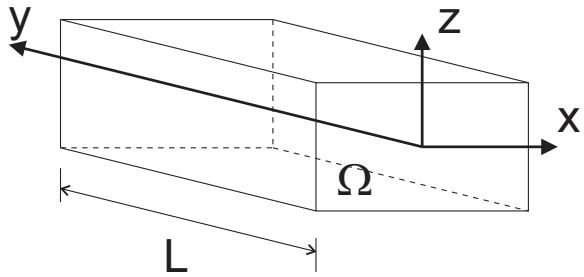

Fig. 1 Beam and adopted Cartesian reference frame

A. Carrera Unified Formulation

Figure 1 shows the Cartesian coordinate system adopted for a generic beam structure. The cross-section Ω is normal to the beam axis y, which has boundaries $0 \leq y \leq L$. It should be highlighted that the validity of the proposed formulation is not affected by the shape of the cross-section and the rectangular cross-section adopted has merely explicative purposes. In the framework of the CUF, the kinematics of a beam model can be summarized as follows:

$$\mathbf{u}(x,y,z) = F_\tau(x,z)\mathbf{u}_\tau(y), \qquad \tau = 1,2,....,M \tag{1}$$

where $\mathbf{u}(x,y,z) = \{u_x(x,y,z) \quad u_y(x,y,z) \quad u_z(x,y,z)\}^T$ is the displacement vector; F_τ indicates the functions of the cross-section coordinates x and z; $\mathbf{u}_\tau$ is the generalized displacement vector; M indicates the number of terms in the expansion. It should be noted that the repeated subscript indicates summation. Moreover, the choice of F_τ and M is arbitrary. Thus, the basis functions adopted to model the displacement field across the section can be different and expanded to any order. For more details about the effects of higher-order terms in the development of refined beam theories within the framework of CUF, the readers are referred to [55].

The models known in the literature as TE (Taylor Expansion) [40, 56] are obtained considering Taylor-like expansion polynomials as F_τ functions. For example, the displacement field of the first-order ($N = 1$) TE model can be expressed as follows:

$$\begin{aligned} u_x &= u_{x_1} + x\, u_{x_2} + z\, u_{x_3} \\ u_y &= u_{y_1} + x\, u_{y_2} + z\, u_{y_3} \\ u_z &= u_{z_1} + x\, u_{z_2} + z\, u_{z_3} \end{aligned} \tag{2}$$

where the parameters on the right-hand side (u_{x_1}, u_{y_1}, u_{z_1}, u_{x_2}, etc.) are the displacements of the

beam axis and their first derivatives. It should be noted that classical beam models, such as EBBM and TBM, are particular cases of the linear TE model above from the kinematic standpoint. However, classical theories and first-order models require the necessary assumption of reduced material stiffness coefficients to correct the Poisson's locking. In this paper, Poisson's locking is corrected according to the method outlined by Carrera et al. [40]. For more details about classical beam theories as particular cases of refined CUF models see [57], where the torsion problem is also considered.

Higher-order terms can be taken into account according to Eq. (1) and higher-order models can be automatically developed by exploiting the hierarchical capability of the TE. For instance, it is clear from the literature that at least a third-order model is needed to correctly guarantee the homogeneity of the shear stresses in the lateral boundaries of the beam (see [58]). This issue is overcome by adopting, for example, the third-order ($N = 3$) TE model.

$$\begin{aligned} u_x &= u_{x_1} + x\, u_{x_2} + z\, u_{x_3} + x^2\, u_{x_4} + xz\, u_{x_5} + z^2\, u_{x_6} + x^3\, u_{x_7} + x^2 z\, u_{x_8} + xz^2\, u_{x_9} + z^3\, u_{x_{10}} \\ u_y &= u_{y_1} + x\, u_{y_2} + z\, u_{y_3} + x^2\, u_{y_4} + xz\, u_{y_5} + z^2\, u_{y_6} + x^3\, u_{y_7} + x^2 z\, u_{y_8} + xz^2\, u_{y_9} + z^3\, u_{y_{10}} \\ u_z &= u_{z_1} + x\, u_{z_2} + z\, u_{z_3} + x^2\, u_{z_4} + xz\, u_{z_5} + z^2\, u_{z_6} + x^3\, u_{z_7} + x^2 z\, u_{z_8} + xz^2\, u_{z_9} + z^3\, u_{z_{10}} \end{aligned} \tag{3}$$

The possibility of dealing with arbitrary expansion makes the TE CUF models able to handle complex problems, such as thin-walled structures and local effects (see [17]).

B. CUF models based on Lagrange polynomials expansions

TE CUF models are characterized by generalized displacements variables (namely, displacements and N-order derivatives of displacements), which lay on the beam reference axis. Recently, a new class of 1D CUF models was introduced in [41], where Lagrange polynomials were adopted as cross-section expanding functions, F_τ. The resulting models are referred to as LE (Lagrange Expansion) and they have only pure displacement variables. Various Lagrange polynomials were used in [41] to develop refined beam theories and some examples are given in Fig. 2. In particular, three-point linear (L3), four-point bi-linear (L4), and nine-point bi-quadratic (L9) polynomials are shown in the picture. The isoparametric formulation was exploited to deal with arbitrary shaped geometries. The Lagrange polynomials can be found in [59]. However, the interpolation functions in the case of

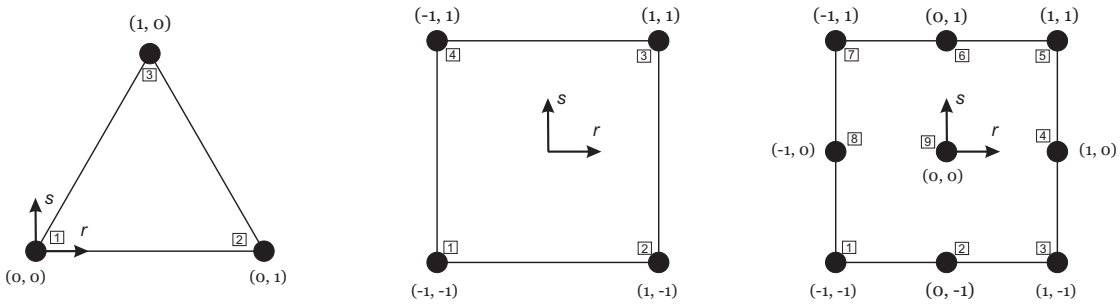

(a) Three-point element, L3 (b) Four-point element, L4 (c) Nine-point element, L9

Fig. 2 Cross-section L-elements in natural geometry

the L9 element are given as an example

$$F_\tau = \tfrac{1}{4}(\mathsf{r}^2 + \mathsf{r}\,\mathsf{r}_\tau)(\mathsf{s}^2 + \mathsf{s}\,\mathsf{s}_\tau) \qquad \tau = 1,3,5,7$$

$$F_\tau = \tfrac{1}{2}\mathsf{s}_\tau^2(\mathsf{s}^2 - \mathsf{s}\,\mathsf{s}_\tau)(1-\mathsf{r}^2) + \tfrac{1}{2}\mathsf{r}_\tau^2(\mathsf{r}^2 - \mathsf{r}\,\mathsf{r}_\tau)(1-\mathsf{s}^2) \qquad \tau = 2,4,6,8 \tag{4}$$

$$F_\tau = (1-\mathsf{r}^2)(1-\mathsf{s}^2) \qquad \tau = 9$$

where r and s vary from -1 to $+1$, whereas r_τ and s_τ are the coordinates of the nine points whose numbering and location in the natural coordinate frame are summarized in Fig. 2c. The displacement field of an L9 beam theory is therefore

$$\begin{aligned} u_x &= F_1\, u_{x_1} + F_2\, u_{x_2} + ... + F_9\, u_{x_9} \\ u_y &= F_1\, u_{y_1} + F_2\, u_{y_2} + ... + F_9\, u_{y_9} \\ u_z &= F_1\, u_{z_1} + F_2\, u_{z_2} + ... + F_9\, u_{z_9} \end{aligned} \tag{5}$$

where $u_{x_1}, ..., u_{z_9}$ are the displacement variables of the problem and they represent the translational displacement components of each of the nine centres of the L9 polynomial. For further refinements, the cross-section can be discretized by using several L-elements as in Fig. 3, where two assembled L9 elements are shown; this is one of the most important characteristics of the CW approach, which is described in Section III.

C. Finite element approximation

The FE approach is adopted to discretize the beam structure along the y-axis (i.e. the longitudinal axis in Fig. 1). This process is accomplished via a classical finite element technique, where

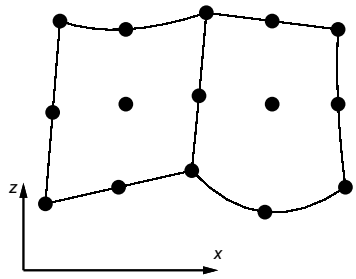

Fig. 3 Two assembled L9 elements in actual geometry

the displacement vector is given by

$$\mathbf{u}(x,y,z) = F_\tau(x,z)N_i(y)\mathbf{q}_{\tau i}, \qquad \tau = 1,...,M,\ i = 1,...,p+1 \tag{6}$$

N_i stands for the shape functions of order p and $\mathbf{q}_{\tau i}$ is the nodal displacement vector,

$$\mathbf{q}_{\tau i} = \left\{ \begin{array}{ccc} q_{u_{x_{\tau i}}} & q_{u_{y_{\tau i}}} & q_{u_{z_{\tau i}}} \end{array} \right\}^{\mathrm{T}} \tag{7}$$

The shape functions are not given here. They can be found in many books, see for example [60]. Elements with four nodes (B4) were adopted in this work, i.e. a cubic approximation ($p = 3$) along the y axis was assumed. The cross-section discretization for the LE class (i.e., the choice of the type, the number and the distribution of cross-sectional Lagrange elements), or of the theory order N for the TE class, are entirely independent of the choice of the beam finite element to be used along the axis of the beam.

The stiffness and mass matrices can be obtained via the principle of virtual displacements; it reads

$$\delta L_{\mathrm{int}} = \int_V \delta\boldsymbol{\epsilon}^{\mathrm{T}}\boldsymbol{\sigma}\,\mathrm{d}V = -\delta L_{\mathrm{ine}} \tag{8}$$

where L_{int} stands for the strain energy; L_{ine} is the work of the inertial loadings; δ stands for the virtual variation; $V = \Omega \times L$ is the volume of the beam; $\boldsymbol{\epsilon}$ and $\boldsymbol{\sigma}$ are the strain and stress vectors, respectively. The virtual variation of the strain energy is rewritten using the constitutive laws, the linear strain-displacement relations, and Eq. (6). It reads

$$\delta L_{\mathrm{int}} = \delta\mathbf{q}_{\tau i}^{\mathrm{T}}\mathbf{K}^{ij\tau s}\mathbf{q}_{sj} \tag{9}$$

where $\mathbf{K}^{ij\tau s}$ is the stiffness matrix in the form of the fundamental nucleus. The derivation of the FE fundamental nucleus of the stiffness matrix is not repeated here for the sake of brevity, but it

is given in [39], where more details about CUF can also be found. However, the components of the stiffness matrix nucleus are provided below and they are referred to as $K_{rc}^{ij\tau s}$, where r is the row number ($r = 1, 2, 3$) and c is the column number ($c = 1, 2, 3$).

$$
\begin{aligned}
K_{11}^{ij\tau s} &= (\lambda + 2G) \int_{\Omega} F_{\tau,x} F_{s,x} \mathrm{d}\Omega \int_{l} N_i N_j \mathrm{d}y + G \int_{\Omega} F_{\tau,z} F_{s,z} \mathrm{d}\Omega \int_{l} N_i N_j \mathrm{d}y + \\
&\quad G \int_{\Omega} F_{\tau} F_{s} \mathrm{d}\Omega \int_{l} N_{i,y} N_{j,y} \mathrm{d}y \\
K_{12}^{ij\tau s} &= \lambda \int_{\Omega} F_{\tau,x} F_{s} \mathrm{d}\Omega \int_{l} N_i N_{j,y} \mathrm{d}y + G \int_{\Omega} F_{\tau} F_{s,x} \mathrm{d}\Omega \int_{l} N_{i,y} N_j \mathrm{d}y \\
K_{13}^{ij\tau s} &= \lambda \int_{\Omega} F_{\tau,x} F_{s,z} \mathrm{d}\Omega \int_{l} N_i N_j \mathrm{d}y + G \int_{\Omega} F_{\tau,z} F_{s,x} \mathrm{d}\Omega \int_{l} N_i N_j \mathrm{d}y \\
K_{21}^{ij\tau s} &= \lambda \int_{\Omega} F_{\tau} F_{s,x} \mathrm{d}\Omega \int_{l} N_{i,y} N_j \mathrm{d}y + G \int_{\Omega} F_{\tau,x} F_{s} \mathrm{d}\Omega \int_{l} N_i N_{j,y} \mathrm{d}y \\
K_{22}^{ij\tau s} &= G \int_{\Omega} F_{\tau,z} F_{s,z} \mathrm{d}\Omega \int_{l} N_i N_j \mathrm{d}y + G \int_{\Omega} F_{\tau,x} F_{s,x} \mathrm{d}\Omega \int_{l} N_i N_j \mathrm{d}y + \\
&\quad (\lambda + 2G) \int_{\Omega} F_{\tau} F_{s} \mathrm{d}\Omega \int_{l} N_{i,y} N_{j,y} \mathrm{d}y \\
K_{23}^{ij\tau s} &= \lambda \int_{\Omega} F_{\tau} F_{s,z} \mathrm{d}\Omega \int_{l} N_{i,y} N_j \mathrm{d}y + G \int_{\Omega} F_{\tau,z} F_{s} \mathrm{d}\Omega \int_{l} N_i N_{j,y} \mathrm{d}y \\
K_{31}^{ij\tau s} &= \lambda \int_{\Omega} F_{\tau,z} F_{s,x} \mathrm{d}\Omega \int_{l} N_i N_j \mathrm{d}y + G \int_{\Omega} F_{\tau,x} F_{s,z} \mathrm{d}\Omega \int_{l} N_i N_j \mathrm{d}y \\
K_{32}^{ij\tau s} &= \lambda \int_{\Omega} F_{\tau,z} F_{s} \mathrm{d}\Omega \int_{l} N_i N_{j,y} \mathrm{d}y + G \int_{\Omega} F_{\tau} F_{s,z} \mathrm{d}\Omega \int_{l} N_{i,y} N_j \mathrm{d}y \\
K_{33}^{ij\tau s} &= (\lambda + 2G) \int_{\Omega} F_{\tau,z} F_{s,z} \mathrm{d}\Omega \int_{l} N_i N_j \mathrm{d}y + G \int_{\Omega} F_{\tau,x} F_{s,x} \mathrm{d}\Omega \int_{l} N_i N_j \mathrm{d}y + \\
&\quad G \int_{\Omega} F_{\tau} F_{s} \mathrm{d}\Omega \int_{l} N_{i,y} N_{j,y} \mathrm{d}y
\end{aligned}
\tag{10}
$$

where G and λ are the Lamé's parameters. If Poisson ν and Young E moduli are used, one has $G = \frac{E}{2(1+\nu)}$ and $\lambda = \frac{\nu E}{(1+\nu)(1-2\nu)}$. The fundamental nucleus has to be expanded according to the summation indexes τ, s, i and j in order to obtain the elemental stiffness matrix.

The virtual variation of the work of the inertial loadings is

$$\delta L_{\text{ine}} = \int_V \rho \delta \mathbf{u}^{\text{T}} \ddot{\mathbf{u}} \, \text{d}V \tag{11}$$

where ρ stands for the density of the material, and $\ddot{\mathbf{u}}$ is the acceleration vector. Equation (11) is rewritten using Eq. (6)

$$\delta L_{\text{ine}} = \delta \mathbf{q}_{\tau i}^{\text{T}} \int_l N_i N_j \text{d}y \int_\Omega \rho F_\tau F_s \text{d}\Omega \, \ddot{\mathbf{q}}_{sj} = \delta \mathbf{q}_{\tau i}^{\text{T}} \mathbf{M}^{ij\tau s} \ddot{\mathbf{q}}_{sj} \tag{12}$$

where $\mathbf{M}^{ij\tau s}$ is the fundamental nucleus of the mass matrix. Its components are provided below in the case of homogeneous material and they are referred to as $M_{rc}^{ij\tau s}$, where r is the row number ($r = 1, 2, 3$) and c denotes column number ($c = 1, 2, 3$).

$$\begin{gathered} \mathbf{M}_{11}^{ij\tau s} = \mathbf{M}_{22}^{ij\tau s} = \mathbf{M}_{33}^{ij\tau s} = \rho \int_l N_i N_j \text{d}y \int_\Omega F_\tau F_s \text{d}\Omega \\ \mathbf{M}_{12}^{ij\tau s} = \mathbf{M}_{13}^{ij\tau s} = \mathbf{M}_{21}^{ij\tau s} = \mathbf{M}_{23}^{ij\tau s} = \mathbf{M}_{31}^{ij\tau s} = \mathbf{M}_{32}^{ij\tau s} = 0 \end{gathered} \tag{13}$$

It is noteworthy that no assumptions about the approximation order have been made in formulating $\mathbf{K}^{ij\tau s}$ and $\mathbf{M}^{ij\tau s}$. It is, therefore, possible to obtain refined beam models without changing the formal expression of the nuclei components. This property of the nuclei is the key-point of CUF that allows, with only nine coding statements, the implementation of any-order of multiple class theories.

The undamped dynamic problem is obtained by substituting the fundamental nuclei into the principle of virtual displacement (Eq. 8), by expanding the CUF fundamental indexes and by assembling the global FEM arrays.

$$\mathbf{M}\ddot{\mathbf{u}} + \mathbf{K}\mathbf{u} = 0 \tag{14}$$

Considering harmonic solutions, the second-order system of ordinary differential equations above results into a classical eigenvalue problem:

$$(-\omega_k^2 \mathbf{M} + \mathbf{K})\mathbf{u}_k = 0 \tag{15}$$

where $\mathbf{u}_k$ is the *k-th* eigenvector.

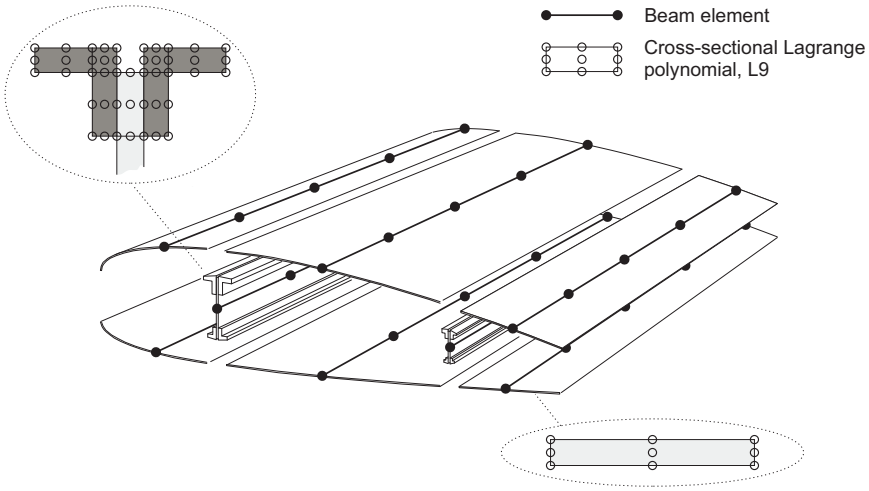

Fig. 4 Component-wise modelling of a sample wing structure

III. Component-wise approach and damage modelling

Recently, LE beam theory has been utilized for the Component-Wise (CW) modelling of complex structures [42–48]. The term CW refers to the fact that Lagrange elements are used to model the displacement variables in each structural component at the cross-sectional level.

Most of the engineering structures are made of different components, such as spar caps, stringers, longerons, ribs and panels in the case of aerospace constructions. However, these components usually have different geometries and scales. Through the CW approach, one can model each typical part of a structure through the 1D CUF LE formulation. In a finite element framework, this means that different components are modelled by means of the same 1D finite element. An example of CW modelling of a typical wing is shown in Fig. 4. According to CW technique, each component of the structure is modelled via beam elements. Then, by exploiting the natural capability of LE to be assembled on the cross-section, Lagrange polynomials (L9 in Fig. 4) are appropriately used to arbitrarily refine the beam kinematics. Compatibilities between the various components is enforced in terms of displacements by superimposing cross-sectional nodes. Alternatively, mathematical techniques might be used, see [61–63]. If a rib were present in the wing in Fig. 4, it would be modelled by beam elements laying on the longitudinal axis, see [42]. One of the main feature of the CW methodology is that it allows for tuning the capabilities of the model by (i) choosing which component requires a more detailed model; and (ii) setting the order of the structural model to be

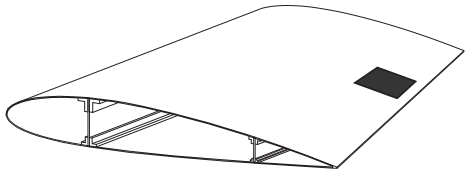

Fig. 5 Locally damaged wing structure

used. Higher-order phenomena (i.e., warping and 3D strain effects) can be, in fact, automatically described by CUF models by opportunely enriching the beam kinematics (see [39]). Moreover, via the CW approach, FE mathematical models can be built by using only physical boundaries; artificial lines (beam axes) and surfaces (plate/shell reference surfaces) are no longer necessary. The numerical assessments detailed in the aforementioned literature, widely demonstrated the capability of the present 1D CW models of dealing with local effects and 3D strain/stress fields. These characteristics are of primarily importance for models to be employed for damage detection through free vibration analysis.

In this paper, a basic isotropic damage modelling approach was adopted. Figure 5 shows an example of locally damaged structure. In the damaged zone, the material characteristics were modified according to the following formula:

$$E_d = d \times E, \text{ with } 0 \leq d \leq 1 \tag{16}$$

where E is the elastic modulus of the material. In other words, Eq. (16) reads

$$E_1 = E;\ E_{0.9} = 0.9 \times E;\ ...;\ E_{0.1} = 0.1 \times E \tag{17}$$

The enhanced capabilities of CUF along with the adopted FE approximation, allow us to arbitrarily place the damage within the structure and evaluate the effects of damage placement and intensity on the free vibration characteristics. It must be underlined, in fact, that the main aim of this paper is to assess and formulate an efficient structural model for the analysis of damaged structures, independently of the damage mathematical characterization. The formulation of more evolute and, eventually, anisotropic damage models is out of the scope of the present research.

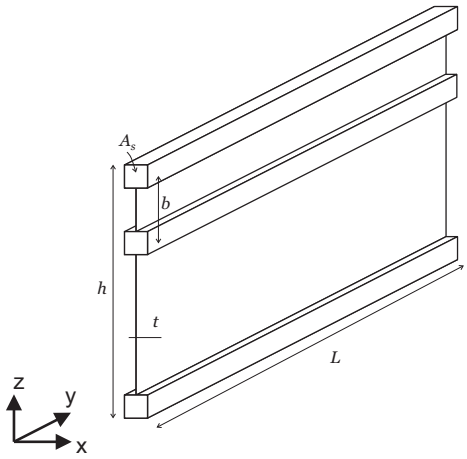

Fig. 6 Three-stringer spar

IV. Numerical Results

A. Three-stringer spar

A simple longeron with three longitudinal stiffeners is discussed as a preliminary test case. The geometry of the spar is shown in Fig. 6 and clamped-free boundary conditions are addressed. The geometrical characteristics of the structure are: length $L = 3$ m; cross-sectional height $h = 1$ m; area of the stringers $A_s = 1.6 \times 10^{-3}$ m^2; thickness of the panels $t = 2$ mm; distance between the middle stringer and the top one $b = 0.3$ m. The longeron is made of an isotropic, homogeneous material with Young modulus $E = 75$ GPa, Poisson ratio $\nu = 0.33$, and density 2700 kg/m^3. The geometrical and material characteristics of the problem were chosen for merely convenience and they do not affect the validity of the following discussion.

Table 1 shows the first 15 natural frequencies of the structure by various theories. Classical (EBBM, TBM), from linear- to fourth-order TE, as well as CW beam models are compared to a detailed MSC Nastran solid model (NAS$_{3D}$) in the table. The results from both TE and CW CUF models were obtained by using 10 B4 elements along the beam axis, which ensured convergent solutions. Regarding the CW model, 5 L9 elements on the beam cross-section were used (one for each component); i.e., a bi-quadratic expansion of the primarily variables on the cross-section of each structural components was assumed. Table 1 also quotes the number of Degrees Of Freedom (DOFs) for each model adopted. A graphical comparison between the first five natural frequencies is provided in Fig. 7, where TBM, second- ($N = 2$) and fourth-order ($N = 4$), CW, and NAS$_{3D}$

	EBBM	TBM	$N=1$	$N=2$	$N=3$	$N=4$	5 L9	NAS_{3D}
DOFs	93	155	279	558	930	1395	3813	62580
f_1	3.24	3.24	3.24	3.43	3.35	3.31	3.46	3.15
f_2	20.29	20.28	20.28	16.70	16.34	16.13	3.52	3.55
f_3	56.81	56.74	56.74	21.39	20.97	20.75	3.76	3.82
f_4	111.36	108.81	108.81	55.25	52.90	51.70	14.27	13.30
f_5	117.60	111.11	111.11	60.11	59.23	58.24	16.73	15.06
f_6	184.30	183.57	183.57	108.19	100.81	97.87	17.67	16.33
f_7	275.94	274.23	269.29	109.44	105.55	102.26	21.17	19.81
f_8	386.89	383.36	274.23	117.79	116.61	113.20	21.71	21.49
f_9	439.21	439.20	383.36	181.03	165.23	119.39	22.95	22.81
f_{10}	517.91	455.17	439.20	194.59	183.16	161.07	25.11	24.07
f_{11}	622.84	511.36	455.17	276.03	197.98	176.65	25.73	24.63
f_{12}	669.05	658.20	511.36	290.25	229.97	189.01	31.21	29.69
f_{13}	830.95	817.28	658.20	325.69	248.76	243.58	37.92	36.24
f_{14}	1104.56	972.68	807.88	393.92	290.54	258.64	45.79	43.88
f_{15}	1317.62	1055.78	817.28	406.78	302.06	281.59	54.86	51.64

Table 1 First 15 natural frequencies (Hz) of the three-stringer spar

models are employed. It is clear that for damage detection and, in general, for the analysis of damaged structures, models able to accurately describe the mechanical behaviour of the structures are needed. Nevertheless, as it was also detailed in [43], classical and refined TE models are able to detect only global modes (e.g., bending and torsional modes). On the contrary, CW refined beam models are able to provide 3D accuracy with very low computational costs. Thanks to CUF and the CW approach, very efficient models able to describe both the local (e.g., shell-like modes) and global modes can be formulated. For illustrative purposes, Fig. 8 shows the first ten vibration modes of the undamaged three-stringer spar by the present CW model. It should be underlined that the 3D mesh in this picture is just a plotting mesh for convenience: the CW models are actually 1D models. From Fig. 8, the higher-order capabilities of the present modelling technique is pretty clear. The CW beam model is, in fact, able to describe the behaviour of the structure at the component

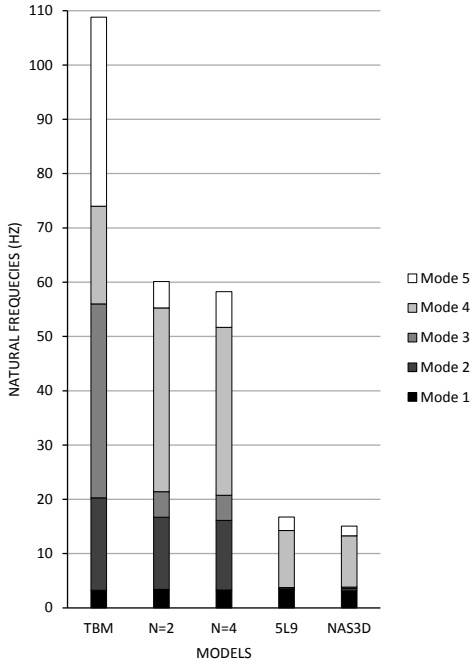

Fig. 7 First five natural frequencies of the three-stringer spar by various models

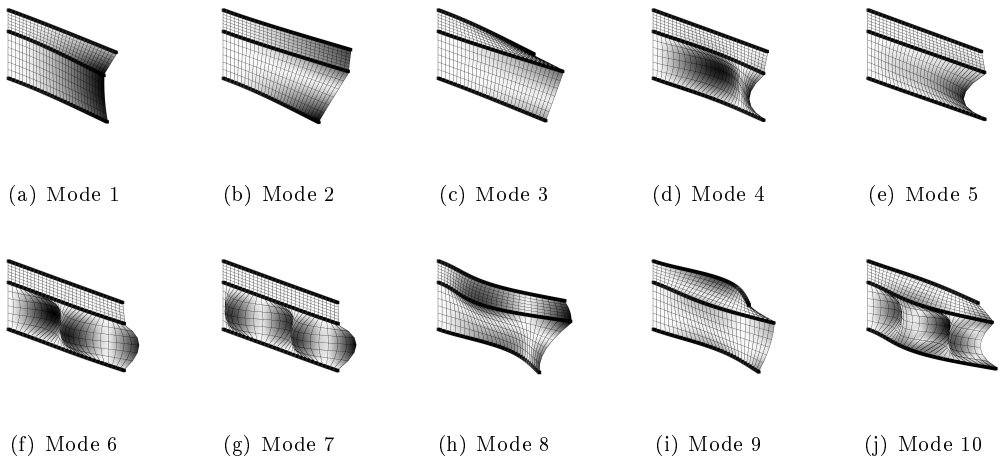

(a) Mode 1 (b) Mode 2 (c) Mode 3 (d) Mode 4 (e) Mode 5

(f) Mode 6 (g) Mode 7 (h) Mode 8 (i) Mode 9 (j) Mode 10

Fig. 8 Mode shapes of the undamaged three-stringer spar; CW model

scale. For this reason, the 5 L9 is used in the following damage analysis.

As detailed in Fig. 9, four damage cases were considered for the structure under consideration. Namely, for damage cases from 1 to 4, the damaged components are, respectively, the top stringer, the top panel, the intermediate stringer, and the bottom panel. The whole components are modelled as damaged, i.e. from the root to the tip.

Table 2 shows the effect of the damage location and intensity on the natural frequencies of the

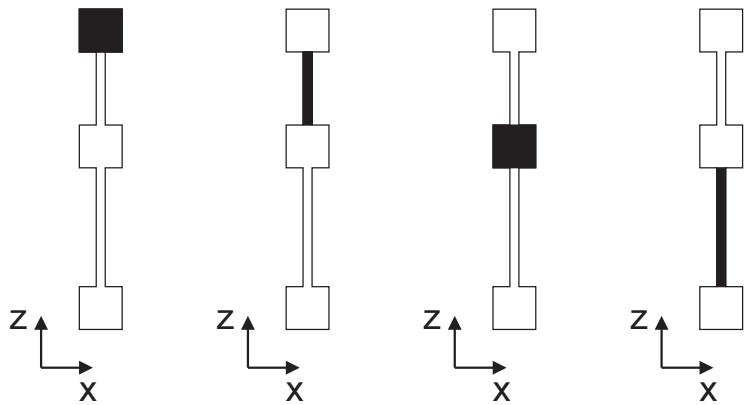

(a) Case 1 (b) Case 2 (c) Case 3 (d) Case 4

Fig. 9 Distribution of the damaged zone on the cross-section of the three-stringer spar; damaged areas in black

longeron. It is clear from the table that the first mode is mainly influenced by the damage in the middle stringer; the second and third natural frequencies is highly affected by damage in the top stringer; higher frequencies are, conversely, sensitive to damage in the lower panel. For each damage case, the effect of damage intensity on the first ten natural frequencies is further investigated in Fig.10 by histograms.

Further investigation was carried out by analysing the effects of damages on the mode shapes by MAC. Figure 11 shows the MAC values between the modes of the undamaged and damaged configurations, for various damage values. The following comments stem from the analysis of the damaged three-stringer spar:

- The free vibration analysis of structures with localized damages demands for accurate models, which are able to describe the mechanics of the structure at the damage level. The CW approach allows us to formulate refined 1D models that replicate solid models solutions with very low computational demand. It represents, therefore, the most efficient and accurate tool for damage analysis of structures and it is used in the remaining part of this work.

- It is important to consider the variation of both natural frequencies and mode shapes for damage analysis and detection. For example, in the case of the three-stringer spar, low damage ($(1-d) = 0.1$) in the top stringer results in a sensible reduction of the 7th natural frequency (approximately 10 %). A similar behaviour is observed for low damage in the intermediate

		Case 1			Case 2			Case 3			Case 4		
$(1-d)$	0	0.1	0.5	0.9	0.1	0.5	0.9	0.1	0.5	0.9	0.1	0.5	0.9
f_1	3.17	3.03	2.66	1.42	3.16	3.15	3.14	$2.79^{\dagger}$	$2.43^{\ddagger}$	$1.36^{\S}$	3.16	3.15	2.97
f_2	3.56	$3.28^{\dagger}$	$3.23^{\ddagger}$	$3.21^{\S}$	3.56	3.56	3.56	3.49	3.47	3.45	3.54	3.53	3.49
f_3	3.83	$3.67^{\dagger}$	$3.66^{\ddagger}$	$3.64^{\S}$	3.78	3.74	3.68	3.77	3.75	3.73	3.82	3.82	3.80
f_4	14.27	14.27	14.26	7.53	14.27	14.26	14.25	13.76	12.87	6.86	$12.39^{\dagger}$	$10.69^{\ddagger}$	$4.94^{\S}$
f_5	16.73	16.73	16.13	14.27	16.73	16.73	16.70	16.71	16.68	15.56	$14.05^{\dagger}$	$11.92^{\ddagger}$	$5.65^{\S}$
f_6	17.67	17.67	16.73	16.73	17.67	17.67	17.67	17.59	17.34	16.23	$14.86^{\dagger}$	$12.60^{\ddagger}$	$5.69^{\S}$
f_7	21.17	18.96	17.67	17.67	21.17	21.17	20.48	19.50	18.06	16.68	$17.73^{\dagger}$	$15.00^{\ddagger}$	$6.72^{\S}$
f_8	21.70	21.17	21.17	20.32	21.67	21.62	21.17	21.15	21.13	20.49	$21.43^{\dagger}$	$18.14^{\ddagger}$	$8.12^{\S}$
f_9	22.95	22.07	22.03	21.17	22.89	22.84	22.62	22.80	22.76	22.32	$21.63^{\dagger}$	$21.56^{\ddagger}$	$9.87^{\S}$
f_{10}	25.10	25.06	25.05	22.00	25.08	25.06	24.89	24.60	24.47	22.75	$22.93^{\dagger}$	$22.07^{\ddagger}$	$11.9^{\S}$
f_{11}	25.75	25.74	25.74	25.04	25.74	25.74	25.70	25.68	25.66	24.35	$24.32^{\dagger}$	$22.90^{\ddagger}$	$14.48^{\S}$
f_{12}	31.21	31.21	31.21	25.74	31.21	31.21	26.87	31.20	31.19	25.49	$26.11^{\dagger}$	$23.84^{\ddagger}$	$17.35^{\S}$
f_{13}	37.92	37.92	37.92	31.21	37.92	37.92	27.89	37.91	37.91	31.11	$31.73^{\dagger}$	$26.82^{\ddagger}$	$20.59^{\S}$
f_{14}	45.79	45.79	44.32	37.92	45.79	45.79	28.17	45.78	43.14	37.76	$38.31^{\dagger}$	$32.38^{\ddagger}$	$21.43^{\S}$
f_{15}	54.85	51.76	45.79	39.27	54.85	52.76	29.56	50.34	45.79	38.79	$45.89^{\dagger}$	$38.79^{\ddagger}$	$22.79^{\S}$

†Most severe damage case for a given vibration mode and $(1-d)=0.1$

‡Most severe damage case for a given vibration mode and $(1-d)=0.5$

§Most severe damage case for a given vibration mode and $(1-d)=0.9$

Table 2 First 15 natural frequencies (Hz) of the three-stringer spar for different damage cases and intensities; 5 L9 CW model

stringer (see Figs. 10a and c). However, the two damage cases can be clearly distinguished by MAC analysis (see Figs. 11a and g). For higher damage intensity ($(1-d)=0.9$), damage cases 1 and 3 can be easily distinguished from merely observing natural frequencies variation (see, for example, the variation of the 5th natural frequency in Figs. 10a and c).

- A damage in the top panel can be detected by observing the first ten natural frequencies only if high damage values are considered. The reason is that local modes involving the top panel, which is smaller than the bottom one, only appear at high frequencies. However, a better estimation of the damage in this case is possible by MAC analysis.

- The considered natural frequencies are mainly affected by damage case 4, i.e. by damage in

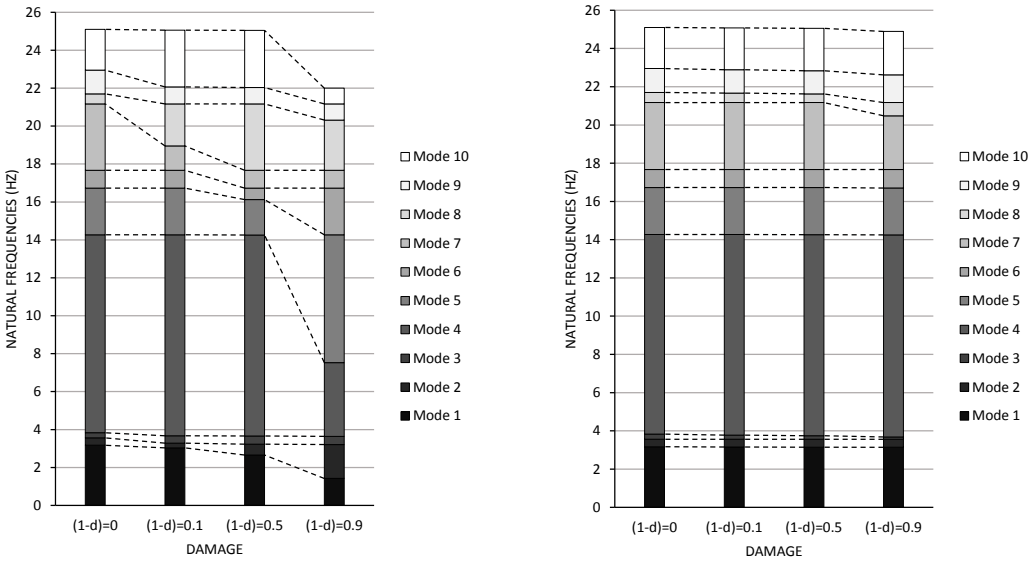

(a) Case 1

(b) Case 2

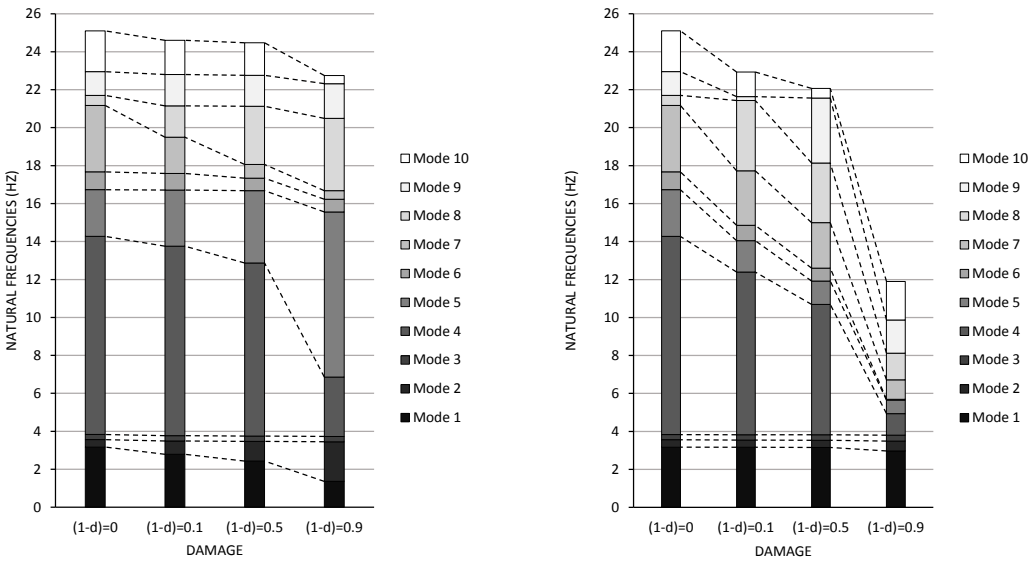

(c) Case 3

(d) Case 4

Fig. 10 Effect of the damage intensity on the first ten natural frequencies of the three-stringer spar; CW model

the lower panel. However, for lower damage intensity, damage location can be confused if only natural frequencies variation is observed (see Fig. 10d). The MAC analysis, on the other hand, allows us to detect bottom panel damage even for lower damage intensity (see Fig. 11j). For example, even for $(1-d) = 0.1$, modes 9 to 11 clearly change with respect to the undamaged

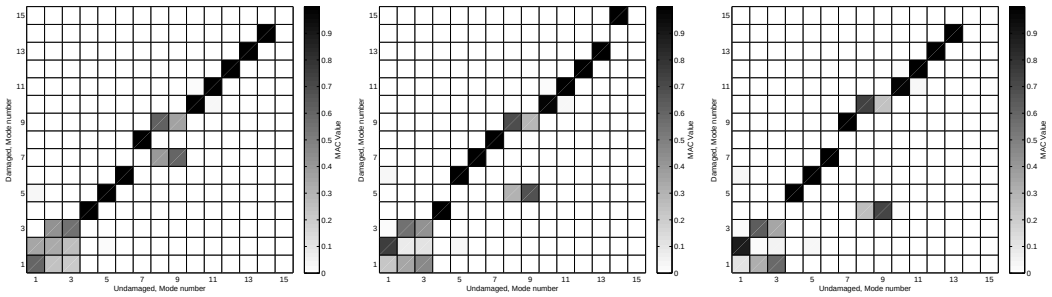

(a) Case 1, $(1-d) = 0.1$ (b) Case 1, $(1-d) = 0.5$ (c) Case 1, $(1-d) = 0.9$

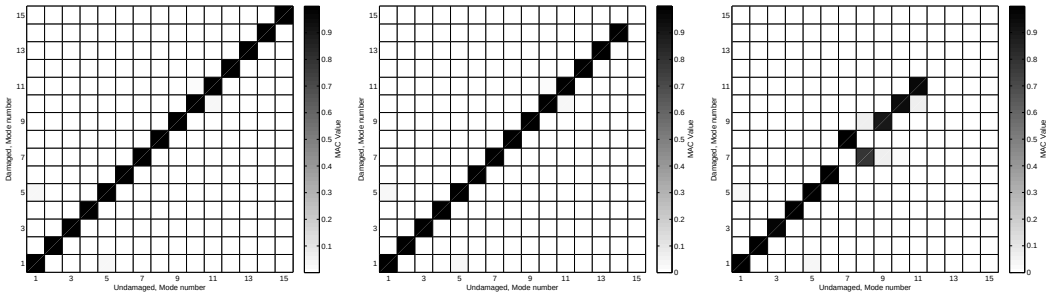

(d) Case 2, $(1-d) = 0.1$ (e) Case 2, $(1-d) = 0.5$ (f) Case 2, $(1-d) = 0.9$

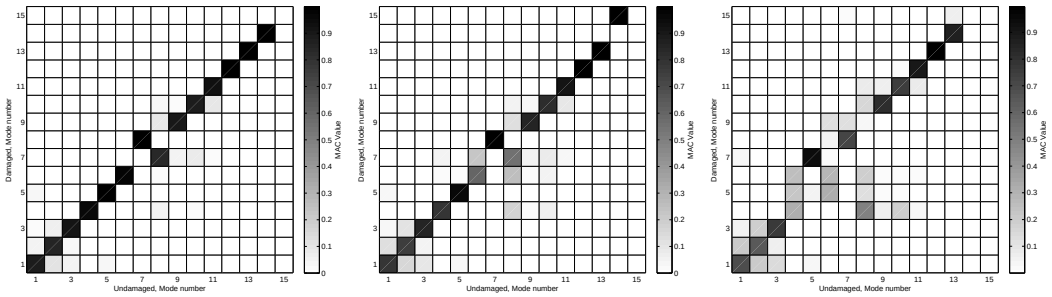

(g) Case 3, $(1-d) = 0.1$ (h) Case 3, $(1-d) = 0.5$ (i) Case 3, $(1-d) = 0.9$

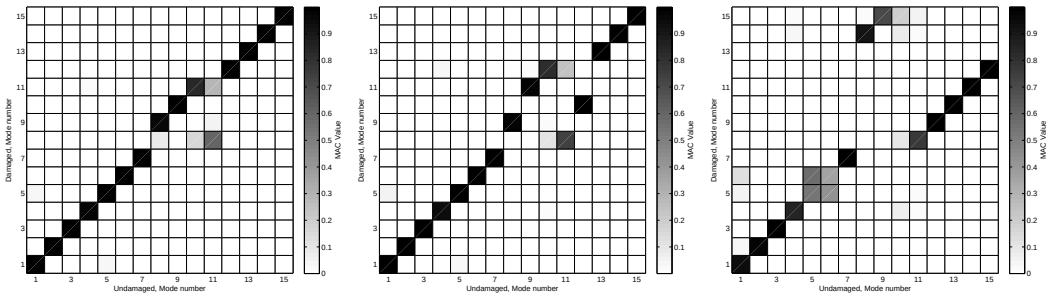

(j) Case 4, $(1-d) = 0.1$ (k) Case 4, $(1-d) = 0.5$ (l) Case 4, $(1-d) = 0.9$

Fig. 11 MAC mode-to-mode comparison between undamaged and damaged three-stringer spar for various damage cases and intensities; 5 L9 CW model

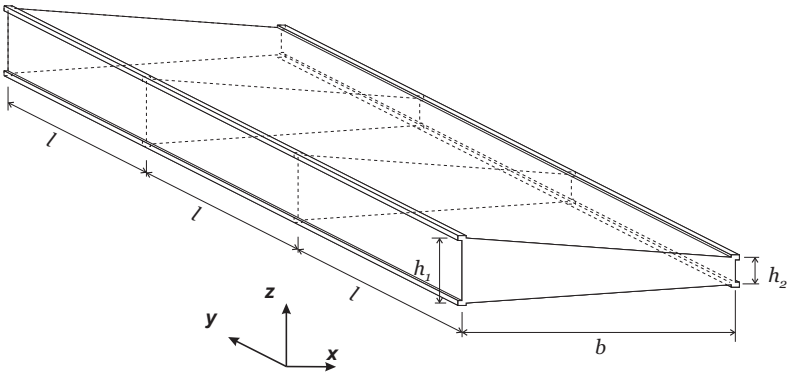

Fig. 12 Three-bay wing box

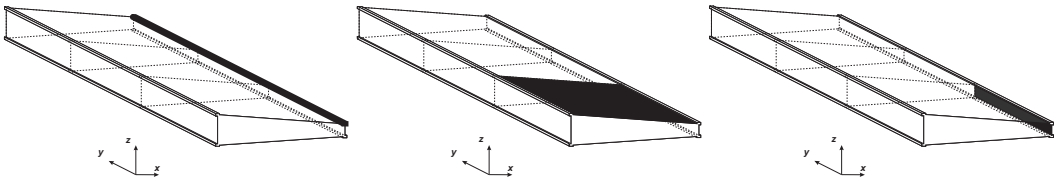

(a) Case 1 (b) Case 2 (c) Case 3

Fig. 13 Damaged zone of the three-bay trapezoidal wing; damaged areas in black

configuration.

B. Three-bay trapezoidal wing box

A three-bay wing box is considered in the second analysis. The same structure was analysed by Rivello [13] and by Carrera et al. [42]. The structure is shown in Fig. 12. The wing consists of three wing boxes each with a length $l = 0.5$ m. The cross-section is a trapezium with height $b = 1$ m. The two webs of the spar have a thickness of 1.6 mm, whereas $h_1 = 0.16$ m and $h_2 = 0.08$ m. The top and bottom panels have a thickness equal to 0.8 mm as well as the ribs. The area of the stringers is $A_s = 8 \times 10^{-4}$ m^2. The wing is completely made of an aluminium alloy 2024, with $G/E = 0.4$ and $\rho = 2700$ kg/m^3.

Figure 13 shows the damage cases considered in the present study. In damage case 1, the top-right stringer is considered as the damaged component; in damage case 2, the top panel close to the clamped end is damaged; and in damage case 3, damage is located in the right web in the first wing box.

Table 3 shows the first 15 natural frequencies of both the undamaged and damaged wings.

		Case 1			Case 2			Case 3		
$(1-d)$	0	0.1	0.5	0.9	0.1	0.5	0.9	0.1	0.5	0.9
f_1	17.78	17.75	17.58	17.23	17.69	13.54	6.09	17.78	17.77	17.77
f_2	18.46	18.44	18.36	18.21	18.10	17.82	16.45	18.46	18.45	18.44
f_3	19.00	19.00	18.99	18.96	18.68	18.57	17.81	19.00	19.00	18.98
f_4	19.12	19.12	19.11	19.09	19.00	18.99	18.56	19.12	19.12	19.12
f_5	19.13	19.13	19.13	19.12	19.13	19.13	18.98	19.13	19.13	19.13
f_6	19.24	19.24	19.24	19.24	19.18	19.17	19.13	19.24	19.24	19.24
f_7	48.01	47.93	47.52	46.86	47.78	36.57	19.17	48.00	47.99	47.97
f_8	49.82	49.77	49.55	49.19	48.86	48.10	34.14	49.82	49.80	49.78
f_9	51.44	51.44	51.42	51.36	50.41	50.09	48.08	51.44	51.44	51.42
f_{10}	51.60	51.60	51.59	51.56	51.44	51.43	50.06	51.60	51.60	51.60
f_{11}	51.65	51.65	51.62	51.58	51.60	51.60	51.42	51.65	51.65	51.65
f_{12}	51.94	51.94	51.93	51.91	51.78	51.77	51.59	51.94	51.93	51.89
f_{13}	70.18	69.72	67.23	62.59	69.91	68.47	51.76	70.04	69.02	63.83
f_{14}	98.20	98.20	97.11	95.67	97.86	75.85	63.31	98.19	98.17	98.13
f_{15}	102.51	102.41	101.88	101.04	101.71	98.38	65.97	102.50	102.47	102.41

Table 3 First 15 natural frequencies (Hz) of the three-bay trapezoidal wing box for different damage cases and intensities; CW model

The results by the 1D CW model are given in the table. The CW model was validated in [42] against classical and refined TE CUF beam models, analytical semi-monocoque solutions from [13], and an MSC Nastran FE model obtained by combining solid and shell elements. It is clear from the published research that the present CW model can overcome the limitations of classical and analytical approaches. In fact, it can reproduce the results of complex FE models with one order of magnitude of DOFs lower and without introducing any geometrical inconsistency in the mathematical model. The CW model used in the present analysis has only 10046 DOFs.

The variation of the first ten natural frequencies versus damage cases and various damage intensities is also graphically depicted in Fig. 14. Finally, Fig. 15 shows the mode-to-mode comparison between undamaged and damaged configurations through a MAC analysis. The analysis suggests

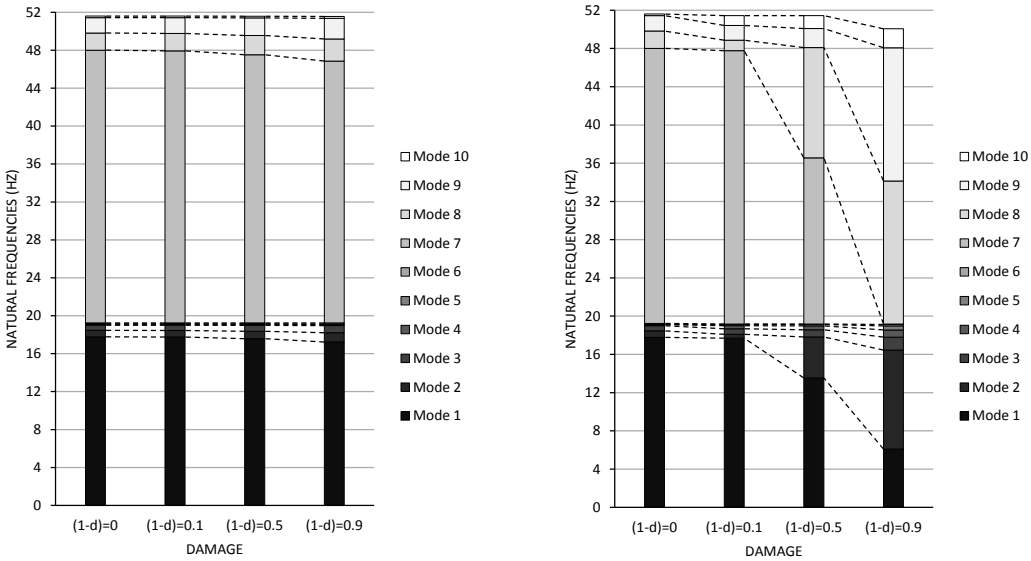

(a) Case 1

(b) Case 2

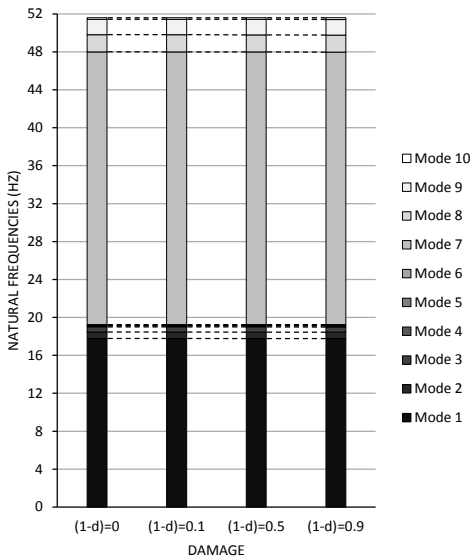

(c) Case 3

Fig. 14 Effect of the damage intensity on the first ten natural frequencies of the three-bay box wing; CW model

the following comments:

- The first 15 modes of the structure are mainly local shell-like modes involving the top and bottom panels of the wing. For this reason, damage cases 1 and 3 do not affect sensibly these modes. In fact, the damage in the stringer is only visible for high damage values (e.g.,

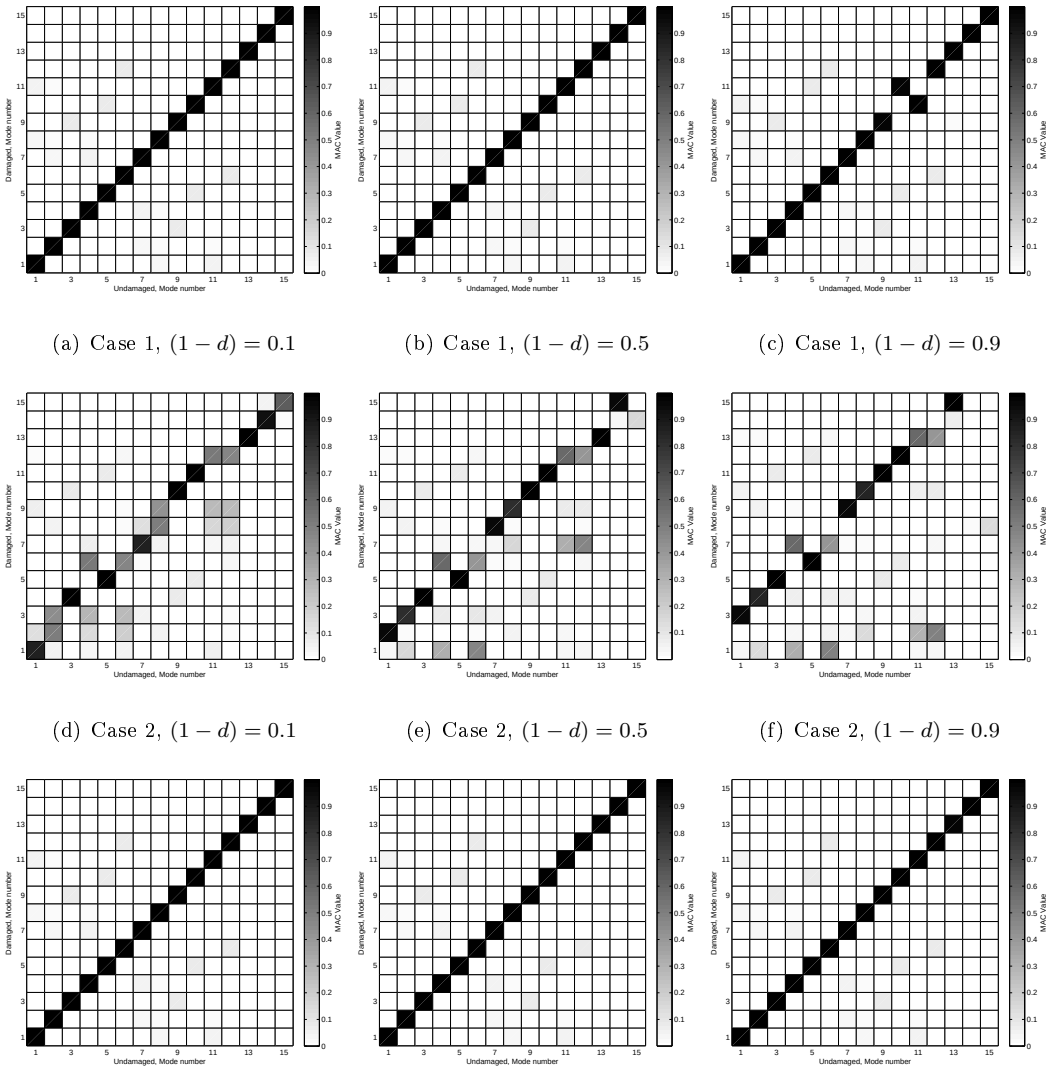

(a) Case 1, $(1-d) = 0.1$ (b) Case 1, $(1-d) = 0.5$ (c) Case 1, $(1-d) = 0.9$

(d) Case 2, $(1-d) = 0.1$ (e) Case 2, $(1-d) = 0.5$ (f) Case 2, $(1-d) = 0.9$

(g) Case 3, $(1-d) = 0.1$ (h) Case 3, $(1-d) = 0.5$ (i) Case 3, $(1-d) = 0.9$

Fig. 15 MAC mode-to-mode comparison between undamaged and damaged three-bay box wing for various damage cases and intensities; CW model

$(1-d) = 0.9$). In this case, a reduction of the value of the 8th natural frequency (Fig. 14a) and a mode exchange in the MAC matrix (10th and 11th modes in Fig. 15c) are observed indeed. Even for high damage values, a damage in the rear web is barely visible in MAC matrices (see Figs. 15g to i). Higher frequency modes should be considered for characterizing damage cases 1 and 3.

- A damage in the top panel (damage case 2) can be easily detected by observing the natural frequencies of the first ten modes (Fig. 14b). In the case of lower damage intensities, a

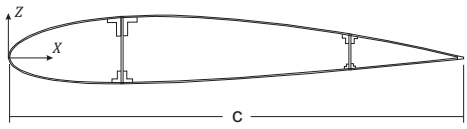

Fig. 16 Cross-section of the NACA profile wing

reduction of the frequencies number 8, 9 and 10 are tangible. For higher damage values, even lower natural frequencies drop.

C. Complete NACA profile wing

A complete wing is considered for the last assessment. The wing, whose cross-section geometry is shown in Fig. 16, is straight with a NACA 2415 airfoil. The chord c is equal to 1 m. The thickness of each panel is 3 mm, whereas the thickness of the spar webs is 5 mm. The cross-sectional dimensions of the spar caps can be found in [43]. The overall length of the structure is $L = 6$ m. The wing is made of three wing boxes, separated by transversal stiffening members at sections $y = 2$ m, 4 m, and 6 m. The thickness of the ribs is equal to 6 mm. For illustrative purposes, the wing is completely metallic and the adopted material is an aluminium alloy with the following characteristics: elastic modulus $E = 75$ GPa; Poisson ratio $\nu = 0.33$; and density $\rho = 2700$ kg/m^3.

Free vibration analyses of the undamaged and various damaged configurations were carried out. Damages were collocated as displayed in Fig. 17. In particular, in the first damage case (Fig. 17a), the whole rear longeron was considered as damaged; in damage case 2 (Fig. 17b), the damage was located in the whole leading edge; the front spar was damaged in case 3 (Fig. 17c); and, finally, damage interested the top central panel in case 4 (Fig. 17d).

The natural frequencies of the undamaged and damaged structure are shown in Table 4. A damage intensity equal to $(1 - d) = 0.5$ was considered. A CW model of the NACA wing was used to list those frequencies. The adopted CW model was obtained by CUF and by employing a combination of L9 elements on the wing cross-section as outlined in [43], where the model was also validated against classical and refined beam theories as well as against complex FEM solutions. For the sake of readability, the first 15 natural frequencies are also given in a graphical form in Fig. 18, where, for each damage case, the variation of the natural frequencies between undamaged

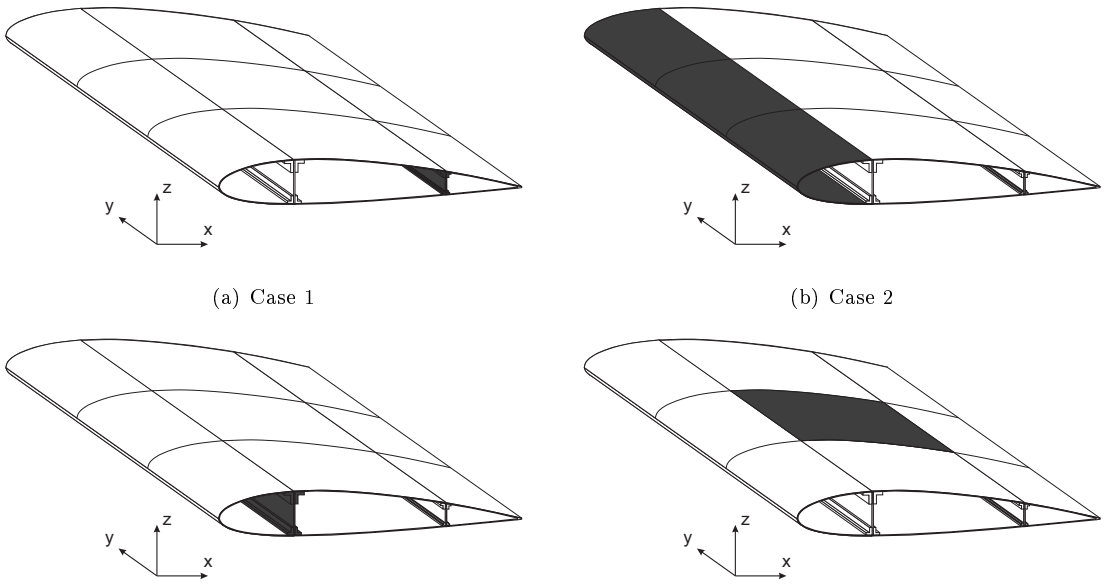

(a) Case 1 (b) Case 2

(c) Case 3 (d) Case 4

Fig. 17 Damaged zones of the NACA profile wing; damaged areas in black

and damaged structure is clearly highlighted.

Some selected mode shapes of the undamaged wing are shown in Fig. 19. Modes 1 to 5 are global modes. Namely, the first mode (Fig. 19a) is the fundamental bending mode in yz-plane; mode 2 (Fig. 19b) is the first bending mode in xy-plane; mode 3 (Fig. 19c) is the second bending mode in yz-plane; mode 4 (Fig. 19d) is a torsional mode; mode 5 (Fig. 19e) is the third bending mode in yz-plane; modes 6 to 15 are local shell-like modes involving top and bottom panels. Mode 9 is shown in Fig. 19f for illustrative purpose.

Mode-to-mode comparisons by MAC between damaged and undamaged structures are shown in Fig. 20 for all the considered damage cases. The following conclusions can be made from the analysis of the NACA wing:

- The damage cases 1, 2 and 3 cannot be detected by comparing the mode shapes between the undamaged and damaged configurations. The MAC matrices in Figs. 20a, b and c show, in fact, an almost perfect correspondence among mode shapes.

- The damage cases 1, 2 and 3 can be distinguished each other by observing the frequencies variation. For example, in case 1, the variation of frequencies 6 to 15 is approximately the same (2-3 %) between undamaged and damage configurations (see Fig. 18a). In case 2, a

	Undamaged	Case 1	Case 2	Case 3	Case 4
f_1	4.14	4.10	3.95	3.42	4.09
f_2	21.28	20.58	19.78	19.18	21.18
f_3	25.00	24.69	23.90	20.59	24.19
f_4	39.45	38.99	36.54	36.49	37.69
f_5	64.84	63.50	62.41	53.74	63.48
f_6	85.61	82.37	84.18	77.28	83.98
f_7	91.54	88.96	89.98	81.13	87.30
f_8	93.46	91.04	92.41	82.84	91.42
f_9	96.99	93.93	94.06	84.86	93.64
f_{10}	103.67	100.98	101.45	94.19	102.34
f_{11}	104.82	102.40	103.09	96.10	104.10
f_{12}	106.76	104.40	105.11	98.13	106.59
f_{13}	109.90	107.11	106.82	99.17	107.80
f_{14}	115.76	112.79	108.78	105.71	114.92
f_{15}	124.19	122.02	121.30	107.38	119.35

Table 4 First 15 natural frequencies (Hz) of the NACA profile wing for different damage cases and $(1-d) = 0.5$; CW model

higher variation of frequency 14 is noticeable (6 %), whereas the other shell-like frequencies behave as in case 1 (see Fig. 18b). In case 3, unlike the the other cases, a variation in global modes is also visible; e.g., 17 % reduction of frequency 5.

- A damage in the top panel (case 4) is clearly detectable by MAC matrix in Fig. 20d, which shows a clear variation in the local mode shapes between the undamaged and damaged structure.

V. Conclusions

This work has proposed advanced one-dimensional models for the free vibration analysis of damaged aircraft structures. Simple spar structures to complete wings have been considered. The analyses were carried out through a Component-Wise (CW) formulation based on the Carrera Uni-

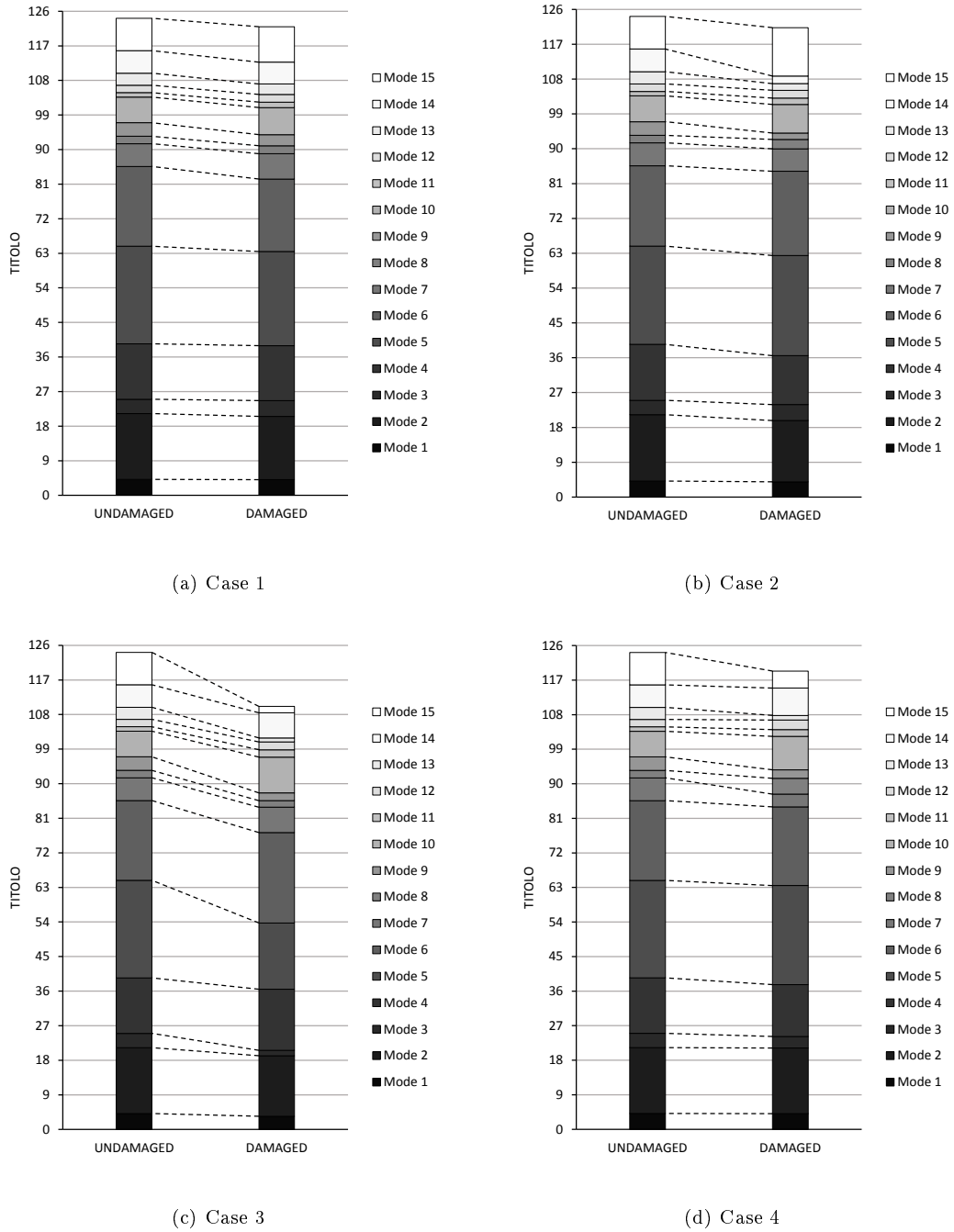

(a) Case 1

(b) Case 2

(c) Case 3

(d) Case 4

Fig. 18 Effect of the damage on the first fifteen natural frequencies of the NACA profile wing; CW model

fied Formulation (CUF). CUF is a tool that allows for the automatic implementation of structural theories by expressing the displacement field as an expansion of the generalized displacements by arbitrary basis functions. If Lagrange polynomials are used, CW models for complex multi-component structures can be easily obtained and opportunely tuned on the basis of the required degree of ac-

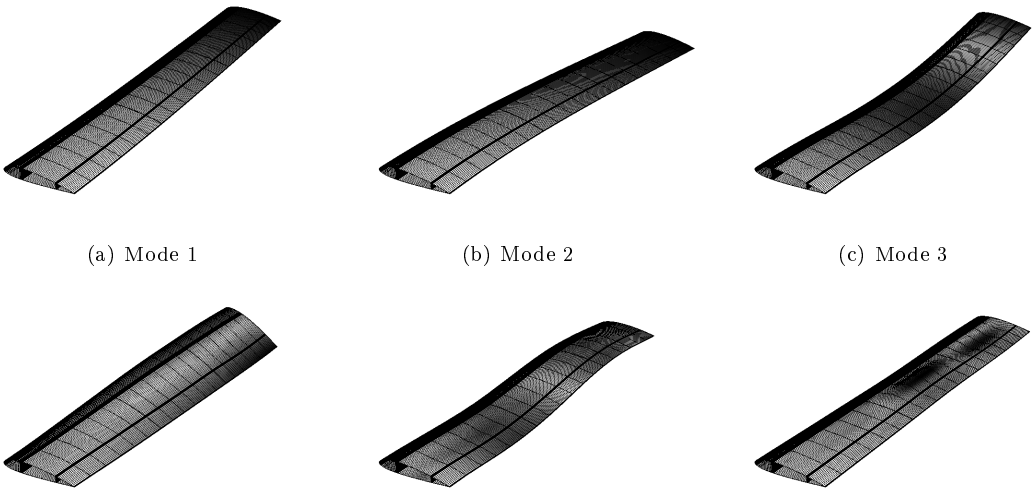

(a) Mode 1 (b) Mode 2 (c) Mode 3

(d) Mode 4 (e) Mode 5 (f) Mode 9

Fig. 19 Mode shapes of the undamaged NACA profile wing; CW model

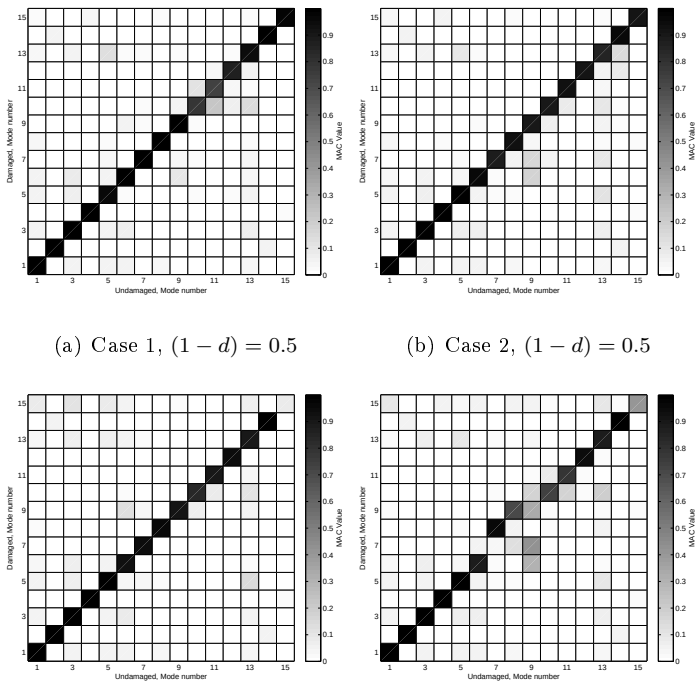

(a) Case 1, $(1-d) = 0.5$ (b) Case 2, $(1-d) = 0.5$

(c) Case 3, $(1-d) = 0.5$ (d) Case 4, $(1-d) = 0.5$

Fig. 20 MAC mode-to-mode comparison between undamaged and damaged NACA profile wing for various damage cases; CW model

curacy. The use of CW features leads to models that provide high-fidelity geometrical and material descriptions of the structure. These are fundamental characteristics demanded for the damage analysis of structures.

In this work, the damage was introduced employing reduced stiffness areas. Globally and locally damaged aircraft structures were considered. The former were damaged along the entire span. The latter has damages in given portions of the span. The effects of damages in various structural components were considered, ranging from damages in the stringer, in the entire longeron and in the panels. The results suggest that

- As known from the previous CUF literature, 1D higher-order models are able to deal with non-classical effects, such as cross-sectional distortions and local effects. The presence of damage worsens the majority of those phenomena. Thus, advanced models are mandatory in damage detection analyses.

- The effect of damage on the natural frequencies and mode shapes depends on the damage location and intensity. It may be very difficult to detect damages within the structure in the case of low damage levels.

- For a given damage, the effects on the free vibrations depend on the mode shapes considered in the analysis. It is important to employ a model able to describe both local and global modes to deal with a wide spectrum of damage cases.

- Natural frequency tracking must be accompanied by mode shapes comparisons in damage detection analyses. In fact, some damage can affect some natural frequencies and not the related mode shapes and vice-versa. MAC is a good tool for mode-to-mode comparison between undamaged and damaged structures.

- The CW approach allows us to deal accurately with damage analysis with very low computational costs. In fact, as known from the previous CUF literature, CW models provide the same accuracy of 3D solid FE analyses with one or two orders of magnitude less DOFs.

The use of CUF models for the analysis of damaged aircraft structures may have interesting outcomes for damage detection. For example, due to its high numerical efficiency and accuracy, CUF and CW models may be employed to create a database of possible damage scenarios to be compared to experimental data, possibly in a CUF-trained neural network.

Acknowledgment

The authors would like to thank Ali Alawami, former undergraduate student in Royal Melbourne Institute of Technology, for his assistance in obtaining some of the results presented in this research.

References

[1] Fayyadh, M., Razak, H., and Ismail, Z., "Combined modal parameters-based index for damage identification in a beamlike structure: theoretical development and verification," *Archives of Civil and Mechanical Engineering*, Vol. 11, No. 3, 2011, pp. 587–609.

[2] Khiem, N. and Toan, L., "A novel method for crack detection in beam-like structures by measurements of natural frequencies," *Journal of Sound and Vibration*, Vol. 333, No. 18, 2014, pp. 4084–4103, doi:10.1016/j.jsv.2014.04.031.

[3] Zhang, Z., Shankar, K., Morozov, E., and Tahtali, M., "Vibration-based delamination detection in composite beams through frequency changes," *Journal of Vibration and Control*, doi:10.1177/1077546314533584.

[4] Capozuzza, R., "Vibration of CFRP cantilever beam with damage," *Composite Structures*, Vol. 116, 2014, pp. 211–222.

[5] Pérez, M., Gil, L., Sánchez, M., and Oller, S., "Comparative experimental analysis of the effect caused by artificial and real induced damage in composite laminates," *Composite Structures*, Vol. 112, 2014, pp. 169–178.

[6] Wang, Y., Liang, M., and Xiang, J., "Damage detection method for wind turbine blades based on dynamics analysis and mode shape difference curvature information," *Mechanical Systems and Signal Processing*, Vol. 48, 2014, pp. 351–367.

[7] Labib, A., Kennedy, D., and Featherston, C., "Free vibration analysis of beams and frames with multiple cracks for damage detection," *Journal of Sound and Vibration*, Vol. 333, No. 20, 2014, pp. 4991–5003.

[8] Nguyen, K., "Mode shapes analysis of a cracked beam and its application for crack detection," *Journal of Sound and Vibration*, Vol. 333, No. 3, 2014, pp. 848–872.

[9] Pollayi, H. and Yu, W., "Modeling matrix cracking in composite rotor blades within VABS framework," *Composite Structures*, Vol. 110, 2014, pp. 62–76, doi:10.1016/j.compstruct.2013.11.012.

[10] Yu, W., Volovoi, V. V., Hodges, D. H., and Hong, X., "Validation of the variational asymptotic beam sectional analysis (VABS)," *AIAA Journal*, Vol. 40, 2002, pp. 2105–2113.

[11] Yu, W. and Blair, M., "GEBT: A general-purpose nonlinear analysis tool for composite beams," *Composite Structures*, Vol. 94, No. 9, 2012, pp. 2677–2689, doi:10.1016/j.compstruct.2012.04.007.

[12] Bruhn, E. F., *Analysis and Design of Flight Vehicle Structures*, Tri-State Offset Company, 1973.

[13] Rivello, R. M., *Theory and analysis of flight structures*, McGraw-Hill, 1969.

[14] Samanta, A. and Mukhopadhyay, M., "Free vibration analysis of stiffened shells by the finite element technique," *European Journal of Mechanics - A/Solids*, Vol. 23, No. 1, 2004, pp. 159 – 179, doi:10.1016/j.euromechsol.2003.11.001.

[15] Euler, L., *De curvis elasticis*, Lausanne and Geneva: Bousquet, 1744.

[16] Timoshenko, S. P., "On the corrections for shear of the differential equation for transverse vibrations of prismatic bars," *Philosophical Magazine*, Vol. 41, 1921, pp. 744–746.

[17] Carrera, E., Pagani, A., Petrolo, M., and Zappino, E., "Recent developments on refined theories for beams with applications," *Mechanical Engineering Reviews*, Vol. 2, No. 2, doi:10.1299/mer.14-00298.

[18] Timoshenko, S. P., "On the transverse vibrations of bars of uniform cross section," *Philosophical Magazine*, Vol. 43, 1922, pp. 125–131.

[19] Timoshenko, S. P. and Goodier, J. N., *Theory of elasticity*, McGraw-Hill, 1970.

[20] Sokolnikoff, I. S., *Mathematical Theory of Elasticity*, McGrw-Hill, 1956.

[21] Cowper, G. R., "The Shear Coefficient in Timoshenko's Beam Theory," *Journal of Applied Mechanics*, Vol. 33, No. 2, 1966, pp. 335–340.

[22] Umanskij, A., *Kručenije i izgib tonkostennykh aviokon-strukcij*, Oborongiz, Moskva, 1939.

[23] Vlasov, V. Z., *Thin-walled elastic beams*, National Science Foundation, Washington, 1961.

[24] Benscoter, S., "A Theory of Torsion Bending for Multicell Beams," *Journal of Applied Mechanics*, Vol. 21, No. 1, 1954, pp. 25–34.

[25] Ladéveze, P. and Simmonds, J., "De nouveaux concepts en théorie des poutres pour des charges et des géométries quelconques," *Comptes Rendus de l'Académie des Sciences de Paris*, Vol. 332, 1996, pp. 445–462.

[26] Berdichevsky, V., "Equations of the theory of anisotropic inhomogeneous rods," *Soviet Physics - Dpklady*, Vol. 21, No. 5, 1976, pp. 286–288.

[27] Hodges, D. H., *Nonlinear Composite Beam Theory*, American Institute of Aeronautics and Astronautics, Reston, Virginia, 2006.

[28] Volovoi, V. V., Hodges, D. H., Berdichevsky, V. L., and Sutyrin, V. G., "Asymptotic theory for static

behavior of elastic anisotropic I-beams," *International Journal of Solid Structures*, Vol. 36, 1999, pp. 1017–1043.

[29] Song, H. and Hodges, D. H., "Rigorous joining of asymptotic beam models to three-dimensional finite element models," *Computer Modeling in Engineering and Sciences*, Vol. 85, No. 3, 2012, pp. 239–278.

[30] Wang, Q. and Yu, W., "A Variational Asymptotic Approach for Thermoelastic Analysis of Composite Beams," *Advances in Aircraft and Spacecraft Science*, Vol. 1, No. 1, 2014, pp. 93–123.

[31] Schardt, R., "Eine Erweiterung der Technischen Biegetheorie zur Berechnung prismatischer Faltwerke," *Der Stahlbau*, Vol. 35, 1966, pp. 161–171.

[32] Schardt, R., *Verallgemeinerte technische biegetheorie*, Springer Verlag, 1989.

[33] Schardt, R., "Generalized beam theory-an adequate method for coupled stability problems," *Thin-Walled Structures*, Vol. 19, 1994, pp. 161–180.

[34] Silvestre, N. and Camotim, D., "First-order generalised beam theory for arbitrary orthotropic materials," *Thin-Walled Structures*, Vol. 40, No. 9, 2002, pp. 791–820.

[35] Giavotto, V., Borri, M., Mantegazza, P., Ghiringhelli, G., Carmaschi, V., Maffioli, G. C., and Mussi, F., "Anisotropic Beam Theory and Applications," *Computers & Structures*, Vol. 16, No. 1–4, 1983, pp. 403–413.

[36] Washizu, K., *Variational Methods in Elasticity and Plasticity*, Pergamon, Oxford, 1968.

[37] Kapania, R. K. and Raciti, S., "Recent Advances in Analysis of Laminated Beams and Plates, Part I: Shear Effects and Buckling," *AIAA Journal*, Vol. 27, No. 7, 1989, pp. 923–935.

[38] Kapania, R. K. and Raciti, S., "Recent Advances in Analysis of Laminated Beams and Plates, Part II: Vibrations and Wave propagation," *AIAA Journal*, Vol. 27, No. 7, 1989, pp. 935–946.

[39] Carrera, E., Cinefra, M., Petrolo, M., and Zappino, E., *Finite Element Analysis of Structures through Unified Formulation*, John Wiley & Sons, 2014.

[40] Carrera, E., Giunta, G., and Petrolo, M., *Beam Structures: Classical and Advanced Theories*, John Wiley & Sons, 2011,
doi:10.1002/9781119978565.

[41] Carrera, E. and Petrolo, M., "Refined Beam Elements with only Displacement Variables and Plate/Shell Capabilities," *Meccanica*, Vol. 47, No. 3, 2012, pp. 537–556,
doi:10.1007/s11012-011-9466-5.

[42] Carrera, E., Pagani, A., and Petrolo, M., "Classical, Refined and Component-wise Theories for Static Analysis of Reinforced-Shell Wing Structures," *AIAA Journal*, Vol. 51, No. 5, 2013, pp. 1255–1268,
doi:10.2514/1.J052331.

[43] Carrera, E., Pagani, A., and Petrolo, M., "Component-wise Method Applied to Vibration of Wing Structures," *Journal of Applied Mechanics*, Vol. 80, No. 4, 2013, pp. 041012/1–15, doi:10.1115/1.4007849.

[44] Carrera, E. and Pagani, A., "Accurate response of wing structures to free vibration, load factors and non-structural masses," *AIAA Journal*. In Press.

[45] Carrera, E., Pagani, A., and Petrolo, M., "Refined 1D Finite Elements for the Analysis of Secondary, Primary, and Complete Civil Engineering Structures," *Journal of Structural Engineering*, pp. 04014123/1–14, doi:10.1061/(ASCE)ST.1943-541X.0001076.

[46] Carrera, E., Pagani, A., and Petrolo, M., "Free vibration analysis of civil engineering structures by component-wise models," *Journal of Sound and Vibration*, Vol. 333, 2013, pp. 4597–4620, doi:10.1016/j.jsv.2014.04.063.

[47] Carrera, E. and Petrolo, M., "Refined One-Dimensional Formulations for Laminated Structure Analysis," *AIAA Journal*, Vol. 50, No. 1, 2012, pp. 176–189. DOI: 10.2514/1.J051219.

[48] Carrera, E., Maiarú, M., and Petrolo, M., "Component-Wise Analysis of Laminated Anisotropic Composites," *International Journal of Solids and Structures*, Vol. 49, 2012, pp. 1839–1851, doi:10.1016/j.ijsolstr.2012.03.025.

[49] Allemang, R. J. and Brown, D. L., "A Correlation Coefficient for Modal Vector Analysis," in "Proceedings of the International Modal Analysis Conference," Orlando, Florida, USA, 1982, pp. 110–116.

[50] Salawu, O. and Williams, C., "Bridge assessment using forced-vibration testing," *Journal of Structural Engineering*, Vol. 121, No. 2, 1995, pp. 161–173.

[51] Zhao, J. and Zhang, L., "Structural Damage Identification Based on the Modal Data Change," *International Journal of Engineering and Manufacturing*, Vol. 4, 2012, pp. 59–66.

[52] Mukhopadhyay, S., Lus, H., Hong, L., and Betti, R., "Propagation of mode shape errors in structural identification," *Journal of Sound and Vibration*, Vol. 331, 2012, pp. 3961–3975.

[53] Balsamo, L., Mukhopadhyay, S., Betti, R., and Lus, H., "Damage Detection Using Flexibility Proportional Coordinate Modal Assurance Criterion," in "Topics in Modal Analysis, Volume 7: Proceedings of the 31st IMAC, A Conference on Structural Dynamics," Conference Proceedings of the Society for Experimental Mechanics Series 45, 2013.

[54] Gopalakrishnan, S., Ruzzene, M., and Hanagud, S., *Computational Techniques for Structural Health Monitoring*, Springer, 2011.

[55] Carrera, E. and Petrolo, M., "On the Effectiveness of Higher-Order Terms in Refined Beam Theories,"

Journal of Applied Mechanics, Vol. 78, 2011, pp. 021013/1–17.

[56] Pagani, A., Boscolo, M., Banerjee, J. R., and Carrera, E., "Exact dynamic stiffness elements based on one-dimensional higher-order theories for free vibration analysis of solid and thin-walled structures," *Journal of Sound and Vibration*, Vol. 332, No. 23, 2013, pp. 6104–6127, doi:10.1016/j.jsv.2013.06.023.

[57] Carrera, E. and Pagani, A., "Evaluation of the accuracy of classical beam FE models via locking-free hierarchically refined elements," *International Journal of Mechanical Sciences*, Vol. 100, 2015, pp. 169–179, doi:10.1016/j.ijmecsci.2015.06.021.

[58] Heyliger, P. R. and N., R. J., "A higher order beam finite element for bending and vibration problems," *Journal of Sound and Vibration*, Vol. 126, No. 2, 1988, pp. 309–326.

[59] Oñate, E., *Structural Analysis with the Finite Element Method: Linear Statics. Volume 1: Basis and Solids*, Springer, Barcelona, 2009.

[60] Bathe, K., *Finite element procedure*, Prentice hall, 1996.

[61] Carrera, E., Pagani, A., and Petrolo, M., "Use of Lagrange Multipliers to Combine 1D Variable Kinematic Finite Elements," *Computers and Structures*, Vol. 129, 2013, pp. 194–206, doi:10.1016/j.compstruc.2013.07.005.

[62] Carrera, E. and Pagani, A., "Analysis of Reinforced and Thin-walled Structures by Multi-line Refined 1D/Beam Models," *International Journal of Mechanical Sciences*, Vol. 75, 2013, pp. 278–287, doi:10.1016/j.ijmecsci.2013.07.010.

[63] Carrera, E. and Pagani, A., "Multi-line enhanced beam model for the analysis of laminated composite structures," *Composites: Part B*, Vol. 57, 2014, pp. 112–119, doi:10.1016/j.compositesb.2013.09.046.